Deletion of PrBP/δ impedes transport of GRK1 and PDE6 catalytic subunits to photoreceptor outer segments

H. Zhang*, S. Li*, T. Doan†, F. Rieke†‡, P. B. Detwiler†, J. M. Frederick*, and W. Baehr*§¶‖

*John A. Moran Eye Center, University of Utah Health Science Center, Salt Lake City, UT 84132; †Department of Physiology and Biophysics and ‡Howard Hughes Medical Institute, University of Washington, Seattle, WA 98195; and Departments of §Neurobiology and Anatomy and ¶Biology, University of Utah, Salt Lake City, UT 84112

The mouse *Pde6d* gene encodes a ubiquitous prenyl binding protein, termed PrBP/δ, of largely unknown physiological function. PrBP/δ was originally identified as a putative rod cGMP phosphodiesterase (PDE6) subunit in the retina, where it is relatively abundant. To investigate the consequences of *Pde6d* deletion in retina, we generated a *Pde6d*$^{-/-}$ mouse by targeted recombination. Although manifesting reduced body weight, the *Pde6d*$^{-/-}$ mouse was viable and fertile and its retina developed normally. Immunocytochemistry showed that farnesylated rhodopsin kinase (GRK1) and prenylated rod PDE6 catalytic subunits partially mislocalized in *Pde6d*$^{-/-}$ rods, whereas rhodopsin was unaffected. In *Pde6d*$^{-/-}$ rod single-cell recordings, sensitivity to single photons was increased and saturating flash responses were prolonged. *Pde6d*$^{-/-}$ scotopic paired-flash electroretinograms indicated a delay in recovery of the dark state, likely due to reduced levels of GRK1 in rod outer segments. In *Pde6d*$^{-/-}$ cone outer segments, GRK1 and cone PDE6α' were present at very low levels and the photopic b-wave amplitudes were reduced by 70%. Thus the absence of PrBP/δ in retina impairs transport of prenylated proteins, particularly GRK1 and cone PDE, to rod and cone outer segments, resulting in altered photoreceptor physiology and a phenotype of a slowly progressing rod/cone dystrophy.

prenyl binding protein | rod/cone dystrophy | vesicular transport | isoprenylation | membrane association

The phototransduction cascade converts light into an electrical signal, thereby initiating vision in photoreceptors of the retina (1, 2). The cascade relies on membrane association of its key components transducin (Tα, -β, and -γ), cGMP phosphodiesterase (PDE6α, -β, and -γ₂), and rhodopsin kinase (GRK1). Membrane association of these proteins is mediated by post-translational N-terminal acylation or C-terminal prenylation (3). The Tα subunits are acylated heterogeneously, the Tγ subunit, PDE6α subunit, and GRK1 are farnesylated (C_{15} side chain), and PDE6β and cone PDE6α' subunits are geranylgeranylated (C_{20} side chain) (for references, see ref. 1). Prenyl side chains are synthesized in all living organisms via the mevalonate pathway and attached to newly synthesized cytosolic proteins carrying a C-terminal CaaX box motif (C, cysteine; a, aliphatic amino acid; X, any amino acid) (4, 5). The prenyl chain is attached to the cysteine of the CaaX motif via a thioether bond by cytosolic prenyl transferases (6). Prenylated proteins dock to the endoplasmic reticulum (ER) and are further processed by ER-associated proteins (7).

Transport of membrane-associated proteins from the ER to the photoreceptor outer segments is inadequately understood. Transport likely involves protein transfer to vesicular carriers and intraflagellar transport mechanisms through the cilium connecting inner and outer segments. Transfer between membranes is thought to be mediated by cytosolic prenyl binding proteins, with a hydrophobic groove accommodating prenyl side chains (5, 7). Posttranslational sorting and targeting of proteins occurs in all cells and is of particular importance in photoreceptors, which renew their entire outer segments roughly every 10 days (8). Because of compartmentalization of inner and outer segments and very active metabolism, photoreceptors are regarded as model cells to study protein trafficking.

PrBP/δ, originally thought to be a subunit of PDE6 and termed PDEδ (9), was shown recently to be a prenyl binding protein (10, 11) and subsequently named PrBP/δ to reflect this fact (12). PrBP/δ orthologs are present in the eyeless *Caenorhabditis elegans* that does not express PDE6 (13), essentially excluding a role of PrBP/δ as PDE6 subunit (see also ref. 12). Genetic and biochemical interaction screens showed that PrBP/δ can interact with prenylated as well as nonprenylated proteins. Interactions with prenylated small GTPases of the Ras superfamily (12, 14–16), with a prenylated prostacyclin receptor, a G protein-coupled receptor located on blood vessels (17), as well as with nonprenylated small GTPases (Arl2 and Arl3) (18) are well established, but the physiological significance of these interactions is largely undefined. In the retina, PrBP/δ was shown to interact *in vitro* with the RCC1-like domain of the retinitis pigmentosa G protein regulator (RPGR) (19, 20), the prenyl chains of rhodopsin kinase (GRK1) (10), and PDE6α and PDE6β subunits (10, 13).

Here, we investigated the consequences of PrBP/δ deficiency on rod and cone photoreceptor function by targeted deletion of its gene in mouse. We show that loss of PrBP/δ does not affect mouse embryogenesis or viability, suggesting that other prenyl binding proteins may substitute for the loss of PrBP/δ. In retina, we found that the expression levels of farnesylated GRK1 and geranylgeranylated cone PDE6 subunits were down-regulated and that these proteins do not transport effectively to the outer segments, thereby affecting photoreceptor physiology and stability.

Results

Generation of *Pde6d*$^{-/-}$ Mice. A *Pde6d*$^{flox/flox}$ mouse line was established by inserting loxP sites flanking exons 2 and 4 of the
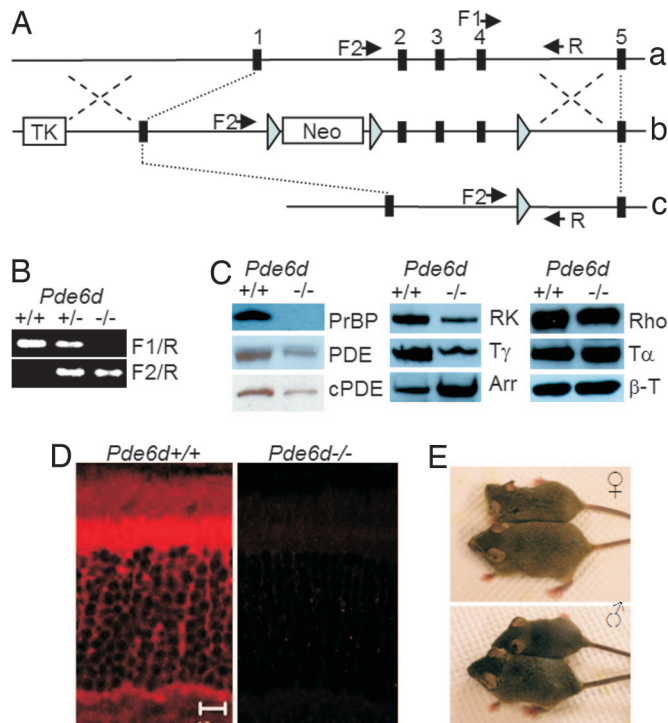
CELL BIOLOGY

Fig. 1. Knockout strategy and phenotype of *Pde6d*⁻/⁻ mice. (*A*) Generation of *Pde6d*⁻/⁻ mice. Structure of the WT *Pde6d* gene (a), the targeting vector (b), and the disrupted *Pde6d* gene (c) are shown schematically. Blue triangles denote loxP, and black rectangles denote exons; F1, F2, and R are primers used for genotyping. TK, thymidine kinase. (*B*) Genotyping of *Pde6d*⁻/⁻ mice by PCR. Amplification with primers PDE6D-F2 and PDE6D-R verified the deletion of sequence between loxP sites. Amplification with primers PDE6D-F1 and PDE6D-R confirmed the WT *Pde6d* allele. (*C*) Immunoblots of 1- to 2-month-old WT and *Pde6d*⁻/⁻ retina lysates. PDE, rod PDE6 catalytic subunits; cPDE, cone PDE6 catalytic subunit; RK, GRK1; Tγ, rod Tγ subunit; Arr, rod arrestin; Rho, rhodopsin; Tα, rod Tα subunit; β-T, β-tubulin as an internal control. Prenylated PDE6 subunits, farnesylated GRK1, and Tγ appear down-regulated, whereas rod arrestin is up-regulated. Acylated Tα and Rho protein levels appear unaffected by deletion of the *Pde6d* gene. (*D*) Labeling of WT and Pde6d⁻/⁻ frozen sections with polyclonal anti-PrBP/δ antibody. Sections were subjected to antigen retrieval (see *Methods*) before blocking and incubating with primary antibody. PrBP/δ (red) is most prominent in the inner segments of rods and cones. (Scale bar: 10 μm.) (*E*) *Pde6d*⁻/⁻ mice (2 months old) were consistently smaller. (*Upper*) Female (−/−) and (+/+) littermates. (*Lower*) Male (+/+) and (−/−) littermates.

Fig. 2. Confocal immunolocalizations of GRK1, rod PDE6, and Tγ in WT (*A*, *C*, and *E*) and *Pde6d*⁻/⁻ (*B*, *D*, and *F*) retina cryosections. (*A* and *B*) Immunoreactivity for GRK1 is prominent over rod and cone outer segments (OS) in WT retina although nearly undetectable in *Pde6d*⁻/⁻ rod and cone OS. (*C* and *D*) Localizations of rod PDE6 in WT and *Pde6d*⁻/⁻ retinas, respectively (MOE antibody; Cytosignal). Rod PDE6 labeling is typically restricted to rod OS in WT retina. Aberrant distribution of rod PDE6 was observed in inner segments and synaptic terminals of *Pde6d*⁻/⁻ rods. (*E* and *F*) Distributions of rod Tγ in WT and *Pde6d*⁻/⁻ retinas, respectively. Tγ mislocalizes, in part, to the inner segment, perinuclear, and synaptic regions (white arrows) of *Pde6d*⁻/⁻ photoreceptors. In each image, propidium iodide (red) demonstrates the extent of the ONL by binding nucleic acids (both DNA and RNA). (Scale bars: 10 μm.) IS, inner segments; OPL, outer plexiform layer.

five-exon gene (Fig. 1*A*). The germ-line *Pde6d*⁻/⁻ mouse was generated by mating the *Pde6d*^flox,flox^ mouse with a CMV-*Cre* transgenic mouse (21). This line expresses *Cre* early during embryogenesis and results in the universal removal of the floxed gene segment. Deletion of the floxed segment was verified by PCR using a primer pair flanking the loxP sites (F2 and R; Fig. 1*B*). Deletion of the *Pde6d* gene was confirmed by immunoblots (Fig. 1*C*) and immunocytochemistry (Fig. 1*D*). Anti-PrBP/δ antibody labeled the WT photoreceptor inner segments intensely, whereas immunolabeling was essentially absent in the *Pde6d*⁻/⁻ retina. The *Pde6d*⁻/⁻ mouse was fertile and developed normally but had 20–30% reduced body weight compared with WT or heterozygous littermates (Fig. 1*E*). Immunoblotting of WT and *Pde6d*⁻/⁻ retina homogenates showed that prenylated phototransduction proteins (PDE, cPDE, and GRK1) were down-regulated in the knockout retinas whereas expression levels of acylated rhodopsin and rod Tα remained largely unchanged (Fig. 1*C*). Interestingly, rod arrestin was up-regulated in the *Pde6d*⁻/⁻ retinas, perhaps to compensate for the decrease
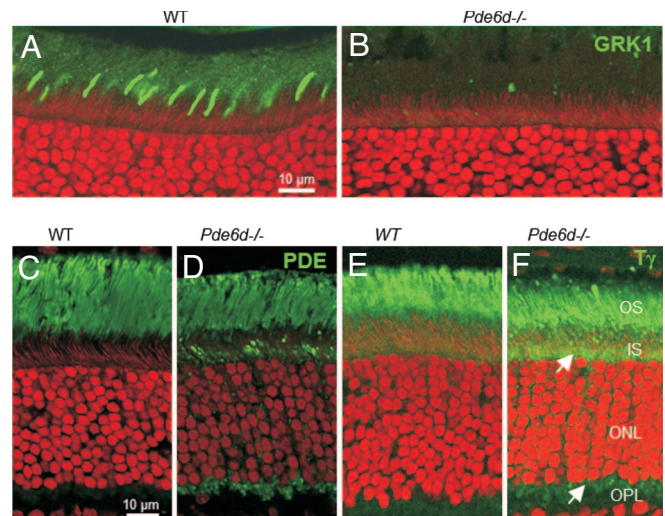
in GRK1 expression in rods, whereas cone arrestin levels were unaffected (data not shown).

Mislocalization of Prenylated Proteins in *Pde6d*⁻/⁻ Rods. The distribution of farnesylated GRK1, known to interact with PrBP/δ strongly (10), was examined in frozen sections of mouse retina. Anti-GRK1 antibody G8 labeled WT photoreceptor outer segments, particularly those of cones (Fig. 2*A*), but surprisingly, immunolabeling was absent in *Pde6d*⁻/⁻ rod and cone outer segments (COS) (Fig. 2*B*). The observed posttranslational down-regulation of GRK1 in the absence of PrBP/δ (Fig. 1*C*) may be due to failed transport and consequent instability. To test this hypothesis, we monitored the stability of GRK1 in retina extracts over a period of 5 h in the presence and absence of recombinant PrBP/δ (supporting information (SI) Fig. 7). The results revealed that GRK1 is labile in the absence of PrBP/δ and that BSA, which does not interact with prenyl groups, could not compensate for the loss of PrBP/δ.

Prenylated catalytic PDE6 subunits were detected predominantly in outer segments of WT rods (Fig. 2*C*), whereas in *Pde6d*⁻/⁻ rods, PDE6 subunits appeared mislocalized to inner segments and within rod spherules (Fig. 2*D*). Rod Tγ, known to be farnesylated (22), was shown to be present in *Pde6d*⁻/⁻ rods but also accumulated perinuclearly and in the myoid region of *Pde6d*⁻/⁻ rod inner segments (Fig. 2 *E* and *F*). The overexpressed rod arrestin distributed throughout the rod cell (SI Fig. 8 *A* and *B*). Other nonprenylated proteins such as rhodopsin (SI Fig. 8 *C* and *D*), Tα subunit (SI Fig. 8 *E* and *F*), guanylate cyclase 1/2, and GCAP1/2 (data not shown) localized normally in *Pde6d*⁻/⁻ rods. These results suggest that transport of GRK1 to the rod outer segment (ROS) is more strongly affected than transport of rod PDE6 subunits.

Cone PDE6α′ Subunits at Low Levels in *Pde6d*⁻/⁻ COS. Cone arrestin is typically observed throughout the somata, in inner and outer
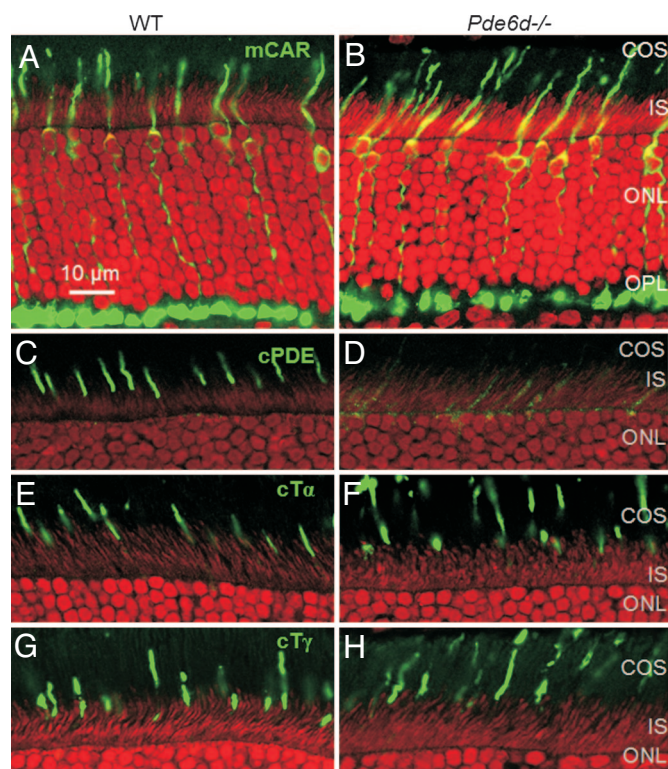
Fig. 3. Localization of cone phototransduction components in WT (*A*, *C*, *E*, and *G*) and *Pde6d*$^{-/-}$ (*B*, *D*, *F*, and *H*) retina sections. In *A* and *B*, cones are labeled from their pedicles to outer segments using anti-cone arrestin antibody. The cone numbers in WT and knockout retinas are comparable at 1–2 months. (*C* and *D*) Labeling with anti-cone PDE6α′ antibody. Cone PDE is nearly absent in *Pde6d*$^{-/-}$ COS but is present at low levels in inner segments. (*E*–*H*) WT and *Pde6d*$^{-/-}$ sections were probed with anti-cone Tα (*E* and *F*) or anti-cone Tγ (*G* and *H*) antibodies. In contrast to geranylgeranylated cone PDEα′, the farnesylated Tα and acylated Tγ subunits show normal distributions in *Pde6d*$^{-/-}$ cones. OS, outer segments; IS, inner segments; OPL, outer plexiform layer.

Fig. 4. Scotopic and photopic ERGs of WT and *Pde6d*$^{-/-}$ mice. (*A* and *B*) Scotopic a- and b-wave amplitudes, respectively, of 2-month-old WT and *Pde6d*$^{-/-}$ mice as a function of light intensity. Error bars represent mean ± SD (*n* = 3–7). (*C* and *D*) Paired-flash ERGs. The intensity of the first and second flash is 1.4 log cd·s·m^{-2}. The interval between two flashes increases from 600 ms to 5 sec. (*E*) Photopic ERG traces of 2-month-old WT and *Pde6d*$^{-/-}$ mice at 0.87 and 2.9 log cd·s·m^2. (*F*) Photopic b-wave amplitudes as a function of light intensity. Error bars represent mean ± SD (*n* = 3–7).

segments, and synaptic pedicles. Immunolocalization of the diffusible cone arrestin appeared comparable in WT and *Pde6d*$^{-/-}$ cones of 1- to 2-month-old littermate mice (Fig. 3 *A* and *B*). *Pde6d*$^{-/-}$ cones did not degenerate to any significant extent at this age (Fig. 3*B*). With regard to outer segment lengths and distributions of ML-opsin and S-opsin, *Pde6d*$^{-/-}$ COS were essentially identical to WT COS (SI Fig. 9). By contrast, cone PDE6α′ could only be detected at low levels in inner and outer segments of the knockout (Fig. 3*D*). Cone Tα (Fig. 3 *E* and *F*) and cone Tγ (Fig. 3 *G* and *H*) were expressed at comparable levels in WT and knockout COS.

Pde6d$^{-/-}$ Photoreceptor Function Assessed by Electroretinogram (ERG). Under scotopic (dim light) conditions, WT a- and b-wave amplitudes increased approximately linearly with increasing flash intensity (Fig. 4 *A* and *B*). The knockout retina produced lower a-wave amplitudes at intensities higher than −1.03 log cd·s·m^{-2} (Fig. 4*A*), whereas the b-wave amplitude decreased at intensities higher than −1.03 log cd·s·m^{-2} (Fig. 4*B*). A double-flash experiment (Fig. 4 *C* and *D*) showed that the *Pde6d*$^{-/-}$ rod b-wave did not recover from the primary flash with interstimulus intervals varying from 600 ms to 5 s. Even after prolonged interstimulus intervals of up to 20 min, the b-wave of the second response never reached its normal amplitude. This observation suggests that the rod cascade is inadequately quenched, most likely because of reduced GRK1 levels in ROS. Under photopic (bright light) ERG conditi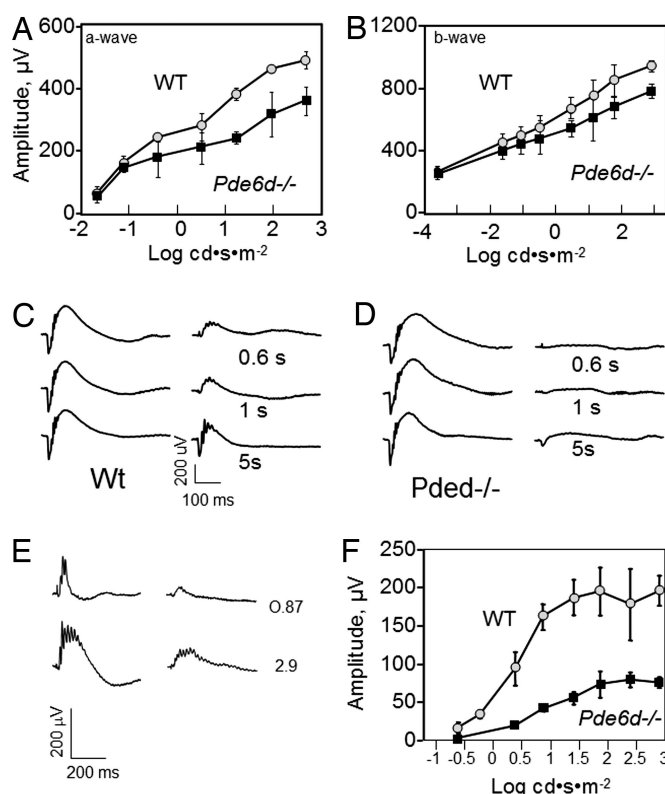ons, the *Pde6d*$^{-/-}$ cone response was strongly diminished (Fig. 4*E*), consistent with reduced PDE6α′ levels in COS. The most intense flash (2.89 log cd·s·m^{-2}) produced a b-wave whose amplitude was approximately one-third of normal (Fig. 4*F*).

Increased Sensitivity of Pde6d$^{-/-}$ Rod Photoreceptors in Single-Cell Recordings. Suction electrodes were used to record outer segment membrane currents of rods from *Pde6d*$^{-/-}$ and control mice. Fig. 5*A* compares average single photon responses for each. Under these conditions, the *Pde6d*$^{-/-}$ responses were larger and longer lasting than those of control rods (time to peak 280 ± 25 ms for 11 *Pde6d*$^{-/-}$ rods, 213 ± 12 for 17 control rods, mean ± SEM). Half-maximal flash strengths were also lower in *Pde6d*$^{-/-}$ rods (Fig. 5*D*).

The differences in sensitivity and kinetics of the *Pde6d*$^{-/-}$ rods could, in principle, be caused by either an increased duration of light-activated PDE activity or a slowing of guanylate cyclase activity. To distinguish between these two possibilities, we measured how the time spent in saturation in response to bright flashes depended on flash strength. Assuming that each saturating response reduces Ca^{2+} to a minimum level and thus creates maximal (and equal) cyclase activity, the time spent in saturation reflects the time required for PDE activity to drop to a threshold level. When the saturation time is plotted against the log of the flash strength, the slope provides an estimate of the time constant for PDE decay. This time constant increased from ≈500 ± 40 msec in control to 655 ± 40 msec in *Pde6d*$^{-/-}$ rods (Fig. 5*C*). Thus, absence of PrBP/δ slowed the decay of light-
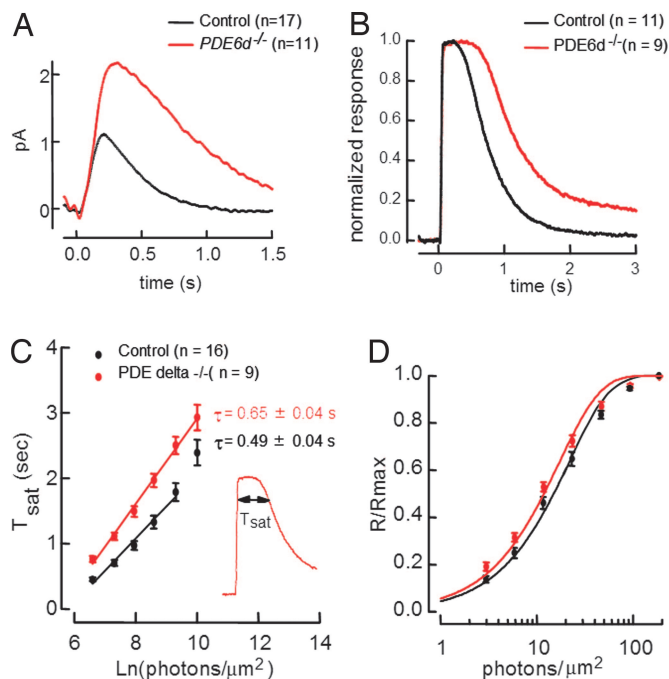
CELL BIOLOGY

Fig. 5. Flash responses in WT and $Pde6d^{-/-}$ single-rod photoreceptors. (A) Average dim flash responses scaled to 1 photoisomerization for WT (n = 17) and $Pde6d^{-/-}$ (n = 11). $Pde6d^{-/-}$ average single-photon response was prolonged relative to WT average single-photon response (time to peak 300 ± 20 vs. 213 ± 12 ms, respectively, mean ± SEM; integration time 736 ± 42 vs. 300 ± 38 ms). (B) Normalized saturating flash responses of WT (n = 11) and of $Pde6d^{-/-}$ (n = 9). $Pde6d^{-/-}$ saturating flash response was prolonged in comparison with WT saturating flash response. (C) Pepperberg plot (delay period T_{sat} for recovery of the dark current vs. log flash intensity) for WT (n = 16) and $Pde6d^{-/-}$ (n = 9). T_{sat} for $Pde6d^{-/-}$ rods was higher than for WT rods at every flash strength measured. Linear regression over the flash strengths measured yielded slopes of 492 ms for WT and 655 ms for $Pde6d^{-/-}$. Error bars represent ± SEM. (D) Mean stimulus response curves of WT (n = 17) and $Pde6d^{-/-}$ (n = 10) with error bars representing ± SEM. Fits are saturating exponential functions, used to estimate the half-saturating flash intensity (WT 14 ± 1 photons per μm², mean ± SEM; $Pde6d^{-/-}$ 13 ± 1 photons per μm²).

activated PDE activity. Because GRK1 is present at very low levels in $Pde6d^{-/-}$ ROS, the retardation may be explained by inefficient rhodopsin phosphorylation.

Retinal Degeneration in $Pde6d^{-/-}$ Mice. We observed a slow degeneration in $Pde6d^{-/-}$ retinas as documented by a shortening of the ROSs as early as 4 weeks of age and a thinning of the outer nuclear layer containing photoreceptor nuclei (ONL) at 5 months of age (Fig. 6 A and B). At 20 months of age, only 3–8 rows of nuclei were present (Fig. 6C). Dark-rearing the mice did not restore outer segment lengths (data not shown), suggesting that this degeneration is unrelated to light damage as observed in $Grk1^{-/-}$ mice (23). Cone photoreceptors could still be identified in the $Pde6d^{-/-}$ retina at 20 months of age (Fig. 6F) but were far fewer, whereas in 2-month-old knockout mice, the cone photoreceptors appear of normal shape and near normal abundance (Fig. 6E). Extrapolated to humans carrying two PDE6D null alleles, the slow progression predicts a phenotype resembling a recessive cone/rod dystrophy. To date, no retina or macular dystrophy has been linked to the human PDE6D gene located on chromosome 2q35-37 (24, 25).

Discussion

PrBP/δ is viewed as a promiscuous, ubiquitous prenyl binding protein whose orthologs have been identified throughout the
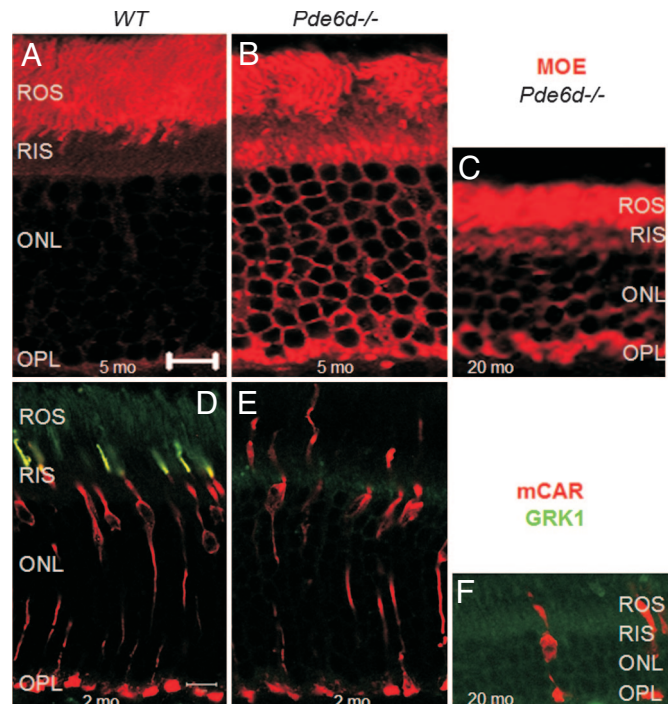

Fig. 6. $Pde6d^{-/-}$ photoreceptor degeneration over time. Localization of rod PDE6 in retina cryosections of 5-month-old WT (A), 5-month-old $Pde6d^{-/-}$ (B), and 20-month-old $Pde6d^{-/-}$ (C) mice is shown. Colocalization of GRK1 (green) and cone arrestin (red) in 2-month-old WT (D), 2-month-old $Pde6d^{-/-}$ (E), and 20-month-old $Pde6d^{-/-}$ (F) retina is also shown. The ONL, consisting of 5–6 rows of photoreceptor nuclei in the knockout, is half that of WT retina at 20 months. RIS, rod inner segments; OPL, outer plexiform layer.

animal kingdom, from unicellular ciliated organisms (*Plasmecium*) and nematodes (*C. elegans*) to humans (SI Fig. 10). Despite the wide distribution of PrBP/δ and the diversity of its targets, deletion of the *Pde6d* gene in mouse did not affect viability, development, and fertility of the animal. The main phenotypes of *Pde6d* deletion are a reduction in body weight of the knockout mouse (Fig. 1E) and transport deficiencies of membrane-associated proteins, particularly GRK1 and cone PDE to COS (Figs. 2B and 3D), which resulted in anomalous photoreceptor physiology (Figs. 4 and 5). The $Pde6d^{-/-}$ ERG responses were less sensitive than the rod responses in single-cell recordings. The a-wave of the ERG provides a good measure of the average amplitude of the rod circulating current and the kinetics of the initial rising phase of the rod light response. However, later components of the rod response are obscured by the b-wave. Thus, the slower and more sensitive rod responses measured with single-cell recordings would not be expected to alter the a-wave of the ERG substantially.

Prenylated Ras, Rab, and Rho GTPases associate posttranslationally with the ER surface (26), where further processing occurs (i.e., proteolytic cleavage of -aaX of CaaX and carboxymethylation). The polypeptides most strongly affected by *Pde6d* deletion, GRK1 and PDE6 subunits, like all other prenylated proteins, are presumed to follow the same pathway and dock to the ER postsynthetically. From there, GRK1 and PDE6 must be targeted to outer segment disk membranes, where phototransduction occurs. We hypothesize that PrBP/δ may be involved in the extraction of prenylated proteins from the ER surface and their subsequent delivery to a vesicular transport carrier. This process is likely regulated by nonprenylated Arf-like (Arl) GTP-binding proteins with which PrBP/δ is known to interact (16). A role of PrBP/δ in transport also corroborates previous *in*

vitro results in which overexpression of PrBP/δ interfered with Ras trafficking from the ER/Golgi to the plasma membrane (15). Polypeptides that fail to transport in the absence of PrBP/δ may be destined for degradation as evidenced by down-regulation of GRK1 in *Pde6d*$^{-/-}$ retina (Fig. 1*C* and Fig. 2 *A* and *B*).

In the PrBP/δ polypeptide, the hydrophobic groove for insertion of prenyl chains is sandwiched between two β-sheet structures (ref. 16; see also SI Fig. 10). By superimposition of protein backbones, it was shown that the hydrophobic pocket can accommodate geranylgeranyl side chains (16). The binding constant of PrBP/δ to geranylgeranyl and farnesyl moieties (K_d of 19.06 and 0.70 μM, respectively) predicts a weaker binding to geranylgeranylated proteins (10). However, geranylgeranylated Pde6α' and farnesylated GRK1 both were nearly undetectable in COS, suggesting that PrBP/δ affects transport of these differentially prenylated proteins similarly. In knockout rods, PDE6 with farnesylated and geranylgeranylated subunits were misrouted in part, but the majority transported to the outer segments (Fig. 2*D*). GRK1 was present at very low levels in *Pde6d*$^{-/-}$ ROS, as shown by immunocytochemistry (Fig. 2*B*), and delay in recovery (Fig. 4 and 5), but farnesylated rod Tγ transported to the *Pde6d*$^{-/-}$ ROS nearly unimpeded, and only a minor portion was retained in the inner segments. These results suggest that deletion of PrBP/δ affects prenylated outer segment proteins distinctly and with some specificity. We hypothesize that specificity of interaction between PrBP/δ and prenylated proteins is governed, apart from prenyl moieties, by additional binding sites on the surface of the proteins that strengthen or weaken interaction.

In cone photoreceptors, GRK1 is presumed to associate with guanylate cyclase-1 (GC1) containing vesicles emerging from the trans-Golgi network (27). In the absence of GC1, GRK1 is undetectable in COS. Interestingly, acylated cone Tα, farnesylated cone Tγ, and geranylgeranylated cone PDE were also undetectable in GC1$^{-/-}$ COS, suggesting that transport of cone transducin and cone PDE also depend on GC1-containing transport carriers. Thus, a mechanism for transport of membrane-associated cone phototransduction proteins is emerging in which PrBP/δ mediates extraction of GRK1 and cone PDE from the ER and delivery to transport vesicles containing the transmembrane protein GC1. In the absence of PrBP/δ, very little GRK1 and insignificant amounts of cone PDE transport to the COS, whereas GC1, its activator guanylate cyclase-activating protein 1 (GCAP1), and cone transducin traffic normally. When GC1 is absent in cones, trafficking of membrane-associated proteins involved in the cGMP cascade is prevented (27).

Parallel studies in the GC1/guanylate cyclase-2 double knockout mouse model have led us to propose that trafficking of membrane-associated proteins follows photoreceptor-distinct pathways. In GC1/guanylate cyclase-2 double knockout rods, PDE is undetectable in ROS, but transducin and GRK1 transport normally (27). In contrast, guanylate cyclase single knockouts do not affect transport of rod PDE. Observation that rod PDE6 localized correctly, in part, to *Pde6d*$^{-/-}$ outer segments predicts alternate mechanisms for extraction of ER-docked prenylated proteins or a redundancy of prenyl binding proteins. Phosducin (*Pdc*), a cytosolic protein which binds to Tβγ subunits once transducin dissociates after light activation of rhodopsin, has been suggested to function as a prenyl binding protein interacting with the farnesyl chain of Tγ (28). In *Pdc*$^{-/-}$ photoreceptors, light-induced translocation of transducin was impeded (29). A second prenyl binding protein candidate is aryl hydrocarbon receptor interacting protein-like 1 (AIPL1), which was shown to be involved in processing of farnesylated PDE6 (30). Knockout of AIPL1, linked to Leber Congenital Amaurosis in humans (31), results in rapid photoreceptor degeneration in the mouse (32). In *Aipl1*$^{-/-}$ photoreceptors, newly synthesized PDE6 does not assemble correctly and is undetectable in ROS,

which suggests a role for AIPL1 in chaperoning ER-docked PDE6 to transport carriers. A third prenyl binding protein candidate is UNC119/HRG4, also expressed ubiquitously and found in photoreceptor inner segments and synaptic terminals (33). Additional and yet unrecognized prenyl binding proteins likely substitute for the loss of PrBP/δ in photoreceptors.

PrBP/δ was recently shown to be instrumental for the internalization and recycling of the human prostacyclin receptor (IP), a G protein-coupled receptor that is farnesylated at its C terminus (17). Prostacyclin acts on platelets and blood vessels and mediates antithrombotic and antiproliferative effects. Internalization of IP represents a GRK/arrestin-independent pathway of desensitization, establishing a physiologically relevant pathway for PrBP/δ outside the retina. Knockdown of PrBP/δ by RNA interference in this system prevented recycling of the receptor in human aortic smooth muscle cells (17). It is unlikely that hypersensitivity of the prostacyclin receptor is responsible for the weight loss observed in the *Pde6d*$^{-/-}$ mouse because the IP$^{-/-}$ mouse shows no morphological abnormalities (34). Presumably, PrBP/δ is involved in systemic metabolism pathways that remain to be explored.

Methods

Generation of the *Pde6d* Knockout Mouse. In the targeting vector, a neo-cassette (*Neo*) flanked by two loxP sequences was inserted in the first intron of the *Pde6d* gene, and another loxP sequence was inserted in intron 4. A thymidine kinase gene was used for negative selection. The targeting vector was used to transform mouse ES cells and generate the ES cells with a floxed *Pde6d* allele by homologous recombination. Replacement of one WT allele by a floxed *Pde6d* allele was confirmed by Southern blotting. One of the engineered ES cell lines was used to produce chimeric mice, completed by the University of Michigan mouse facility. The chimeric mice were mated with WT C57BL/6 mice (purchased from Charles River, Wilmington, MA). Two lines of chimeric mice successfully transmitted the floxed *Pde6d* to produce heterozygous mice with one WT *Pde6d* allele and one floxed *Pde6d* allele. Mice transmitting the floxed *Pde6d* allele in the germ line were mated with transgenic mice expressing *Cre recombinase* (*cre*) driven by the CMV promoter (21) (Jackson Laboratory, Bar Harbor, ME). Primers F1 (5′-GTCAGTAACTGCCACCTAACC) and R (5′-GGACTTTCGGTGTCGTTCAC) were used to identify WT and floxed alleles by PCR. Mice carrying a disrupted *Pde6d* allele were bred further to produce homozygous *Pde6d* knockout mice without the *cre* gene. Primers specific for the *cre* gene were used to track the segregation of the *cre* gene from the *Pde6d* knockout mice. Primers F2 (5′-CACTGAGCCATCTCTCCAGTG) and PDE6D-R were used to verify the deletion of sequence between loxP sites (Fig. 1*B*).

Immunoblotting. Immunoblotting was performed as described (35). The following antibodies were used: anti-PrBP/δ and anti-PDE6β polyclonal antibodies (R. Cote, University of New Hampshire, Durham, NH); anti-GRK1 monoclonal antibody (G8; K. Palczewski, Case Western Reserve University, Cleveland, OH); anti-cone opsin (Chemicon, Temecula, CA); anti-rhodopsin (1D4; R. Molday, University of British Columbia, Vancouver, BC, Canada); anti-cone Tα (Cytosignal Research Products, Irvine, CA); anti-mouse cone arrestin (LUMI-J) and rod arrestin (C10C10) polyclonal antibodies (C. Craft, University of Southern California, Los Angeles, CA); anti-rod PDE6αβγ antibody (Cytosignal, Irvine, CA); anti-cone PDE6α' (T. Li, Harvard Medical School, Boston, MA); and anti-rod Tα (UUTA) and anti-rod Tγ antibodies (C. K. Chen, Virginia Commonwealth University, Richmond, VA).

Confocal Immunolocalization. Age-matched mouse eyes were cautery-marked for orientation, immersion-fixed, and processed as described (27). Sections were viewed by using a Zeiss (Thorn-

wood, NY) LSM 510 inverted Laser Scan confocal microscope using a ×40, 1.3 N.A. oil objective lens and optical slit setting of <0.9 μm. Images were taken consistently inferior to the optic nerve of each section.

Antigen Retrieval. Cryosections (12 μm thick) were placed on charged glass slides. PrBP/δ immunolabeling was improved by washing retina cryosections in PBS (twice for 5 min) to remove the TBS embedding medium and by immersing the slides in a coplin jar containing preheated 10 mM sodium citrate solution (pH 6.0) at 88°C. The coplin jar was placed in a beaker containing boiling water for 10 min. After rinsing briefly with distilled water three times and with PBS once, the sections were incubated with anti-PrBP/δ antibody overnight at 4°C, reacted with secondary antibody, and imaged.

ERGs. Before recording, mice were dark-adapted overnight and anesthetized by i.p. injection using 60 mg ketamine and 10 mg xylazine per kilogram of body weight. ERGs were recorded by using a UTAS E-3000 (LKC Technologies, Inc., Gaithersburg, MD) apparatus. The pupil was dilated by applying a drop of 1% tropicamide to the subject eye for 10–15 min. For scotopic ERGs of WT mice, the recovery time between each flash varied from 10 to 60 sec (depending on the flash intensities) at low intensities ≤0.39 log cd·s·m^{-2}. For test flash intensities >0.39 log cd·s·m^{-2}, the recovery interval between two flashes was >2 min. For scotopic ERGs of $Pde6d^{-/-}$ mice, the recovery time intervals between flashes varied from 20 sec to 5 min when the flash intensities were 0.39 log cd·s·m^{-2} or less. For knockout mice subjected to more intense light, each knockout mouse was used only once for the high-intensity light flash test because of extremely long time required for photoreceptors to recover fully. For paired flashes, both the test and probe flashes were 1.4 log cd·s·m^{-2} with intervals varying from 600 ms to 5 sec. For photopic ERGs, the recordings were performed under a back-ground light of 1.48 log cd·s·m^{-2}; the stimulating flash intensity varied from −0.61 to 2.89 log cd·s·m^{-2}.

Single-Cell Recordings. WT and $Pde6d^{-/-}$ single-rod-cell recordings were performed as described (36). In brief, a mouse was dark-adapted overnight, and the retinas were isolated under infrared light. A small piece of retina was shredded, and the resulting suspension was transferred to a recording chamber and superfused with Ames solution warmed to 37°C. Suction electrodes were used to record the light-sensitive current from single ROSs. Under our recording conditions, the rod's single photon responses reach peak later and have a larger amplitude than previously reported. Correspondingly, the time constant for PDE decay is longer than that previously reported. The reason for these differences is unknown.

GRK1 In Vitro Protection Assay. Two fresh $Pde6d^{-/-}$ retinas were homogenized in 400 μl PBS with 1 mM DTT and the homogenate was divided equally. To one sample, 20 μg of recombinant PrBP/δ was added, and to the other, 20 μg BSA was added. The samples were incubated at 0°C for 30 min and then at 37°C. A 30-μl aliquot was removed at indicated time points, mixed with equal volume of 2× SDS gel loading buffer, and frozen. Ten microliters of retina extract were blotted and probed with anti-GRK1 antibody (G8).

1. Burns ME, Arshavsky VY (2005) *Neuron* 48:387–401.
2. Lamb TD, Pugh EN, Jr (2006) *Invest Ophthalmol Vis Sci* 47:5138–5152.
3. Hancock JF, Cadwallader K, Paterson H, Marshall CJ (1991) *EMBO J* 10:4033–4039.
4. Magee T, Seabra MC (2005) *Curr Opin Cell Biol* 17:190–196.
5. McTaggart SJ (2006) *Cell Mol Life Sci* 63:255–267.
6. Zhang FL, Casey PJ (1996) *Annu Rev Biochem* 65:241–269.
7. Gelb MH, Brunsveld L, Hrycyna CA, Michaelis S, Tamanoi F, Van Voorhis WC, Waldmann H (2006) *Nat Chem Biol* 2:518–528.
8. Besharse JC, Hollyfield JG (1979) *Invest Ophthalmol Vis Sci* 18:1019–1024.
9. Gillespie PG, Prusti RK, Apel ED, Beavo JA (1989) *J Biol Chem* 264:12187–12193.
10. Zhang H, Liu XH, Zhang K, Chen CK, Frederick JM, Prestwich GD, Baehr W (2004) *J Biol Chem* 279:407–413.
11. Zhang H, Hosier S, Terew JM, Zhang K, Cote RH, Baehr W (2005) *Methods Enzymol* 403:42–56.
12. Norton AW, Hosier S, Terew JM, Li N, Dhingra A, Vardi N, Baehr W, Cote RH (2005) *J Biol Chem* 280:1248–1256.
13. Li N, Baehr W (1998) *FEBS Lett* 440:454–457.
14. Marzesco AM, Galli T, Louvard D, Zahraoui A (1998) *J Biol Chem* 273:22340–22345.
15. Nancy V, Callebaut I, El Marjou A, de Gunzburg J (2002) *J Biol Chem* 277:15076–15084.
16. Hanzal-Bayer M, Renault L, Roversi P, Wittinghofer A, Hillig RC (2002) *EMBO J* 21:2095–2106.
17. Wilson SJ, Smyth EM (2006) *J Biol Chem* 281:11780–11786.
18. Hanzal-Bayer M, Linari M, Wittinghofer A (2005) *J Mol Biol* 350:1074–1082.
19. Linari M, Ueffing M, Manson F, Wright A, Meitinger T, Becker J (1999) *Proc Natl Acad Sci USA* 96:1315–1320.
20. Linari M, Hanzal-Bayer M, Becker J (1999) *FEBS Lett* 458:55–59.
21. Schwenk F, Baron U, Rajewsky K (1995) *Nucleic Acids Res* 23:5080–5081.
22. Hagiwara K, Wada A, Katadae M, Ito M, Ohya Y, Casey PJ, Fukada Y (2004) *Biochemistry* 43:300–309.
23. Chen CK, Burns ME, Spencer M, Niemi GA, Chen J, Hurley JB, Baylor DA, Simon MI (1999) *Proc Natl Acad Sci USA* 96:3718–3722.
24. Li N, Florio SK, Pettenati MJ, Rao PN, Beavo JA, Baehr W (1998) *Genomics* 49:76–82.
25. Lorenz B, Migliaccio C, Lichtner P, Meyer C, Strom TM, D'Urso M, Becker J, Ciccodicola A, Meitinger T (1998) *Eur J Hum Gen* 6:283–290.
26. Hancock JF (2003) *Nat Rev Mol Cell Biol* 4:373–384.
27. Baehr W, Karan S, Maeda T, Luo DG, Li S, Bronson JD, Watt CB, Yau K-W, Frederick JM, Palczewski K (2007) *J Biol Chem* 282:8837–8847.
28. Lukov GL, Hu T, McLaughlin JN, Hamm HE, Willardson BM (2005) *EMBO J* 24:1965–1975.
29. Sokolov M, Sguanylate cyclase-2sel KJ, Leskov IB, Michaud NA, Govardovskii VI, Arshavsky VY (2004) *J Biol Chem* 279:19149–19156.
30. Ramamurthy V, Roberts M, van den AF, Niemi G, Reh TA, Hurley JB (2003) *Proc Natl Acad Sci USA* 100:12630–12635.
31. Sohocki MM, Bowne SJ, Sullivan LS, Blackshaw S, Cepko CL, Payne AM, Bhattacharya SS, Khaliq S, Qasim MS, Birch DG, et al. (2000) *Nat Genet* 24:79–83.
32. Ramamurthy V, Niemi GA, Reh TA, Hurley JB (2004) *Proc Natl Acad Sci USA* 101:13897–13902.
33. Kobayashi A, Kubota S, Mori N, McLaren MJ, Inana G (2003) *FEBS Lett* 534:26–32.
34. Murata T, Ushikubi F, Matsuoka T, Hirata M, Yamasaki A, Sugimoto Y, Ichikawa A, Aze Y, Tanaka T, Yoshida N, et al. (1997) *Nature* 388:678–682.
35. Zhang H, Cuenca N, Ivanova T, Church-Kopish J, Frederick JM, MacLeish PR, Baehr W (2003) *Invest Ophthalmol Vis Sci* 44:2858–2867.
36. Howes KA, Pennesi ME, Sokal I, Church-Kopish J, Schmidt B, Margolis D, Frederick JM, Rieke F, Palczewski K, Wu SM, et al. (2002) *EMBO J* 21:1545–1554.